Bicarbonate Buffers Can Promote Crosslinking and Alternative Gas-phase Dissociation Pathways for Multiprotein Complexes

Gongyu Li,[†, Π, §, $] Junfeng Huang,[†] Zhen Zheng,[†] Qinjingwen Cao,[‡] Yuwei Tian,[Π #] Guangming Huang,[§] Lingjun Li[†,‡] and Brandon T. Ruotolo[*,Π]

[†] School of Pharmacy and [‡]Department of Chemistry, University of Wisconsin-Madison, Madison, WI, 53705, USA

[Π] Department of Chemistry, University of Michigan, Ann Arbor, Michigan 48109-1055, United States

[§] Department of Chemistry, School of Chemistry and Materials Science, University of Science and Technology of China, Hefei Anhui, 230026, P. R. China

[$] Present Address: Research Center for Analytical Science, College of Chemistry, Nankai University, Tianjin 300071, P. R. China

[#] Present Address: Eli Lilly and Company, 893 Delaware St, Indianapolis, IN 46225

[*] corresponding author:
Brandon T. Ruotolo:
E-mail: bruotolo@umich.edu
Phone: 734-615-0198

ORCID:
G.L. - 0000-0002-2367-4433
L.L. - 0000-0003-0056-3869
B.T.R - 0000-0002-6084-2328

Abstract

Previously, we have reported the stabilization effect of Hofmeister salts for multiprotein complexes (MPC) in the absence of bulk solvent (*J. Am. Chem. Soc.* **2011,** *133* (29), 11358-11367; *Angew. Chem. Int. Ed.* **2012,** *51* (23), 5692-5695; *Angew. Chem. Int. Ed.* **2013**, *52* (32), 8329-8332.). Our efforts sought to bridge the gap between gas-phase protein structures and those found in solution. To reveal more detailed MPC topology information, native ion mobility-mass spectrometry (IM-MS) measurements are often combined with gas-phase activation methods. Conventional activation methods, including collision induced dissociation/unfolding (CID/CIU), however, primarily report information focused on monomeric subunits within the MPC, limiting the topological information obtained. Herein, we describe a simple buffer-doping method that promotes an alternative MPC CID pathway which readily produces product ions that correspond to larger sub-complexes from within some parent assemblies. Interestingly, tetramers exhibiting a dimer of dimers quaternary structure (e.g. hemoglobin and concanavalin A) produce dimeric product ions upon collisional activation following ionization from bicarbonate buffer, in contrast to the commonly observed monomer-ejection CID pathway. In order to both further investigate and validate our native IM-MS, we performed bottom-up proteomics experiments on MPCs housed in bicarbonate buffer. Our efforts revealed evidence of bicarbonate-mediated disulfide bond formation in proximal Cystine residues. We close by discussing the applications for these observations in the context of MPC structure determination by native IM-MS.

1. Introduction

Higher order structures of multiprotein complexes (MPCs) are a key determinative factor for their functions *in vivo*. For example, hemoglobin (Hb), a centrally-important heme-containing MPC involved in oxygen transport and renal dysfunction following rhabdomyolysis, is highly conserved [1, 2]. As is typical for MPCs, the dynamic assembly and disassembly of Hb in solution involves several comprehensive and reversible steps. It is argued that hetero-tetrameric Hb dissociates into hetero-dimeric globin (αβ) in acetate buffer at a pH above 6.5, which is followed by a further dissociation of dimeric globin into single chain (α- and β-globin) concomitant with heme group detachment at a pH below 5 [3]. Konermann *et al.* observed a similarly dimeric globin-driven dissociation pathway in solution from freshly obtained Hb which is free of oxidative damage [4]. These solution architectures, combined with mass spectrometry (MS)-derived residue-level noncovalent contact information and many other structural biology tools including X-ray crystallography and cryoEM, provides a structural basis for Hb biological function of oxygen transport. Despite these and other efforts aimed at elucidating Hb dynamics [5-7], there remain many unanswered questions surrounding the interplay between Hb structure, function and subunit exchange.

Native ion mobility-mass spectrometry (IM-MS) is rapidly becoming a versatile tool for accessing protein assembly processes and topological information [8-11]. To explore the structure of proteins and MPCs, desolvation is a required step. In general, this step is accomplished using nano-electrospray ionization (nESI), and is believed to generate MPC ions that resemble their native states in the solution phase. In addition to direct measurements of MPC mass (accomplished using MS) and collision cross-section (CCS) (accomplished using IM) of MPCs, additional organizational and sequence-level information can be obtained using gas-phase protein activation. For example, collision induced dissociation (CID) and collision induced unfolding (CIU) have emerged as widely used methods for detailed MPC structure interrogation [12-14]. The resultant MPC dissociation and unfolding patterns can often be correlated to native protein structures and properties [13, 15, 16].

Although multiple strategies have emerged for utilizing gas-phase information in the construction of native-state models of MPCs [6, 17-22], the dissociation pathways accessed by MPC ions upon CID contrast sharply with the known solution structures of such assemblies. For example, CID of Hb, a 64 kDa hetero-tetramer comprised of homo-dimers, exhibits evidence of classical asymmetric ejection of unfolded monomeric units, in contrast to expectations derived from the native quaternary structure of the MPC, which is organized as a dimer-of-dimers [3]. Notably, MPC charge state has been demonstrated experimentally and theoretically to have a profound effect on gas-phase dissociation and unfolding [15, 23]. To pave the way for the development of native IM-MS for the characterization of MPCs of increasing size and complexity, activation techniques must be improved in order to provide needed details surrounding MPC structure and dynamics that remain refractory to other structural probes [24].

Chemical crosslinking, in combination with MS (especially in the context of bottom-up proteomics), has emerged as a useful strategy to capture transient protein-protein interactions and to map protein-protein interaction interfaces at an unprecedented scale [25, 26]. Previous efforts have been devoted to developing multi-functional MS-cleavable crosslinkers with different spacer arms ranging from zero to more than 24 Å in length [27-29]. For example, bismaleimide sulfoxide reagents with spacer arms of 24.2 Å target cystine residues and permit the assessment of protein-protein interactions with distance constraints as long as ~45 Å to be captured as a result of the protein backbone flexibility [30]. Our previous work has revealed the stabilization effects of MS-cleavable cross-linkers [31], tags [32, 33],

anions [19], and cations [18] on MPCs, as well as their influence on MPC CID [17]. Here, we describe a simple buffer-doping approach to promote alternative CID pathways for MPCs. In our experiments, ammonium bicarbonate (NH_4HCO_3) is added to native protein solutions prior to nESI. We explore the effect of this additive both in solution and in the gas phase using top-down/tandem MS, bottom-up LC-MS/MS, CIU fingerprints, pH measurements and circular dichroism (CD) spectroscopy. Based on this collection of evidence, we propose a tentative mechanism that relies upon the promotion of disulfide bonds in proximal Cysteine residues within bicarbonate buffers. These additional non-specific yet structurally-informative disulfide bonds promote both more compact MPC structures in the gas-phase and alternative CID pathways. For example, disulfide-linked dimerization between α- and β-chain monomers within Hb was observed experimentally using LC-MS/MS. Such precursors go on to produce dimeric product ions upon CID. We conclude by exploring the implications of our observations for native IM-MS in the context of MPC structure discovery.

2. Experimental

Chemicals. Protein standards including concanavalin A (jack bean, ConA), glutamate dehydrogenase (GDH) and alcohol dehydrogenase (ADH, *Saccharomyces cerevisiae*), transthyretin (human, TTR), and bovine serum albumin (BSA) were purchased from Sigma-Aldrich. Protein standard samples were buffer exchanged into 100 mM ammonium acetate buffer using Micro Bio-Spin 30 columns (Bio-Rad, Hercules, CA) without further purification. All solvents used in this study were of HPLC grade. No further purifications were performed for all reagents. Purified water (conductivity of 18.2 MΩ.cm) was obtained from Milli-Q® Reference System (Millipore Corp., USA).

Hemoglobin Sample Treatments. Hemoglobin was dissolved in 100 mM NH_4OAc to make a stock solution of 10 mg/mL. A volume of 2.5 μL hemoglobin stock solution was mixed with certain volume of 100 mM NH_4OAc and 1 M NH_4HCO_3 solution to make a total volume of 92.5 μL. Seven conditions were tested for hemoglobin treatments covering absence/presence of NH_4HCO_3 and different temperatures. Each treatment has three sample replicates. No NH_4HCO_3 was used in treatment 1-3 which was performed at room temperature, 37 °C and 50 °C, respectively. On the other hand, 2.5 μL NH_4HCO_3 solution was added in treatment 4-6 which was performed at room temperature, 37 °C and 50 °C, respectively. 5 μL NH_4HCO_3 solution was used in treatment 7 where treatment temperature was at 50 °C. After 10 min heating process in water bath, sample was digested with 1 μL 0.5 mg/mL trypsin (Promega, WI, USA) at 37 °C for 17 hours then desalted with Agilent Omix C18 tips and dried down in vacuum.

Circular dichroism (CD) characterization. CD measurements were performed on a Jasco J-810 CD spectrometer. The CD spectra were recorded from 280 to 190 nm. The blank spectrum was also recorded on the buffer for baseline corrections. Protein samples after heating was quickly transferred to CD cell and then acquired the spectrum as soon as possible. All experiments were repeated three times, and the average values were used in analyses.

Bottom-up LC-MS analysis. All instrumental experiments were performed using a Q Exactive HF Hybrid Quadrupole-Orbitrap mass spectrometer (Thermo Fisher Scientific) coupled with a Dionex Ultimate 3000 UPLC with 0.1% formic acid (FA) water as mobile phase A and 0.1% FA ACN as mobile phase B. Samples were dissolved in 12.5 μL 0.1% FA H_2O and centrifuged for 10 μL supernatant collection. 1 μL sample was injected each time into a C18 column (75 μm × 15 cm, 1.7 μm) self-packed with 150 Å, BEH C18 material from a Waters column (part no. 186004661). Samples were loaded with 3% B and further separated by the gradient linearly ramped to 40% B in 40 min. The

gradient then ramped to 75% B in another 0.5 min and kept for 10 min, later ramped to 97% B in another 0.5 min and kept for 10 min, and then the column was equilibrated with 3% B for 12 min. The MS analysis was performed in data-dependent mode which utilizes HCD to fragment the most abundant 15 ions with spray voltage of 2.25 kV and capillary temperature of 325 °C. Full MS scans were acquired with resolution of 60 K, AGC target of 1e6 and maximum injection time of 150 ms. MS/MS spectra were generated under normalized collision energy of 30, with isolation width of 1.3 *m/z*, resolution of 15 K, AGC target of 1e5, maximum injection time of 150 ms and dynamic exclusion of 45 s.

Label-free quantification of disulfide peptide from bulk-heated hemoglobin. The theoretical masses of disulfide-linked peptide with different charges (+5, +6, +7 and +8) were calculated and their EIC peak areas in each sample were summed and normalized to TIC revealing distinct abundance levels across different treatments as shown in Figure 4d. For peptide identification, the high-resolution MS1 and corresponding MS/MS spectra were used to annotate peptide fragments.

ConA protein heating and digestion. ConA protein samples were separated into four groups with exactly the same protein concentration and buffer (100 mM ammonium acetate, pH 6.8), and then treated with four different conditions: 1) control group without bicarbonate and no heating (sitting in room temperature), 2) with additional heating but no bicarbonate, 3) with 25 mM bicarbonate and heating, and 4) with 50 mM bicarbonate and heating. All heating experiments are carried out using a dry bath, with temperature keeping at 37 ºC for 10 minutes. After heating treatments under different conditions, 20 µl of each treated ConA samples were taken out to perform the tryptic digestion. Adding to each sample was 1 µg sequencing grade trypsin (Promega, Madison, WI) with a protein to enzyme ratio at 20:1, and the mixtures were incubated at 37 ºC for 16 h. The digestion were quenched by acidifing the tryptic peptides with trifluoracetic acid (TFA). Prior to LC-MS/MS analysis, all samples need to desalt with Sep Pak C18 cartridge (Waters, Milford, MA) following standard protocols provided by the vendor.

ConA nanoLC-MS/MS analysis. Desalted samples were analyzed with an Ultimate 3000 nanoLC coupled to an Orbitrap Fusion Lumos Tribrid mass spectrometer (Thermo Fisher Scientific, San Jose, CA). Re-dissolved the sample with 0.1% FA and loaded onto a 75 mm i.d. × 18 cm length homemade column with 1.7 µm, 130 Å, BEH C_{18} material from a Waters UPLC column (Waters, Milford, MA). Peptides were separated with a gradient that started from 97% solvent A (0.1% FA in H_2O) and 3% solvent B (0.1% FA in ACN) to 30% solvent B over 25 min and then kept each of 85% solvent B and 100% solvent A for 10 min. The flow rate was set at 300 nL/min. MS method was set according to the following parameters: MS: scan range (*m/z*) = 300-2000; resolution = 120,000; AGC target = $1.0e^6$; maximum injection time = 100 ms; included charge state = 2-8; dynamic exclusion duration = 10 s. MS/MS method is a top 20 data-dependent acquisition (DDA) mode in which all MS/MS dissociations were performed with higher energy collisional dissociation (EThcD): resolution = 60,000; ETD reaction time (+2, 50ms; +3-4, 25ms; +5, 15ms; +6-8, 10ms); ETD Reagent Target =$2.0e^5$; Max ETD Reagent injection time = 200 ms; AGC target =$2.0e^5$; Max injection time = 200 ms; HCD collision energy = 33%.

ConA data processing. Acquired MS raw files were analyzed using Byonic software (Protein Metrics, San Carlos, CA) and searched against ConA protein sequence (Uniprot ID P02866). Precursor ion mass tolerance of 10 ppm and fragment ion mass tolerance of 0.01 Da were selected. The deamidation of asparagine (N) and glutamine (Q) and the oxidation of methionine (M) were set as variable modifications. Peptide identifications were filtered at 1% two-dimensional false discovery rate (2D

FDR), Byonic Score > 150, Delta Modification Score > 10, and PEP2D < 0.01. To relatively quantify the abundance of deamidation in the identified peptides, we used the Xcalibur Browser (Thermo Fisher Scientific, San Jose, CA) to calculate the peak area of each identified peptide peak with or without deamidation in the MS chromatogram for comparison. The total peak area of a peptide with and without deamidation is regarded as 100%, and the percentage of each deamidation form is calculated by dividing the peak area of one deamidation form by the total peak area.

CIU-IM-MS experiments. A quadrupole ion mobility time-of-flight mass spectrometer (Synapt G1, Waters, Milford, MA, USA) was used for all ion mobility experiments. Approximately 5 µL of each sample were loaded into nanospray source and MS instrument was run in positive ion mode. Nanospray voltages range between 1.0-2.0 kV and the sampling cone was used at 30 V. The Synapt instrument was tuned to allow preservation and transmission of native proteins and protein interactions. This typically involves elevated pressures in the source region (~4 mbar), and decreasing all focusing voltages (e.g., cone, extractor, and bias voltages). The traveling-wave ion mobility separator was operated at a pressure of ~3.5 mbar, and DC voltage waves (30 V wave height traveling at 400 m/s) to generate ion mobility separation. The ToF-MS was operated over the *m/z* range of 400-8000. CCS calibration curves were generated using a previously described protocol, and using literature CCS values derived for use with the Synapt instrument platform [34, 35]. CIU was achieved by increasing the trap CE from 10-160V with a step voltage of 10V.

CIU Data analysis. To generate the CIU fingerprints, only the data at *m/z* values corresponding to the selected charge state of the precursor ions were selected for analysis. We used CIUSuite to process CIU data as published previously [36]. Once the amount of parent oligomer was less than five percent of the total signal, we terminated the experiment. The data were normalized at each voltage through dividing the intensities of ions at each drift time by the maximum ion intensity observed at that voltage.

3. Results and Discussion

Previous reports have elucidated the disassembly of Hb tetramers in solution, produced upon decreasing solution pH or increasing temperature, which involves the evolution of Hb dimers (Left panel in **Scheme 1**) which eventually decay into monomeric globin chains [4, 5, 37-39]. A close inspection of the Hb structure reveals a dimer-of-dimers quaternary structure [38], which promotes the dimer dissociation pathway described above by virtue of the smaller protein surface contact areas that exist between dimers than are present within dimers. In contrast, Hb CID experiments (Right panel in **Scheme 1**), result in the direct ejection of unfolded Hb monomers, with little evidence of dimeric CID product ions [3].

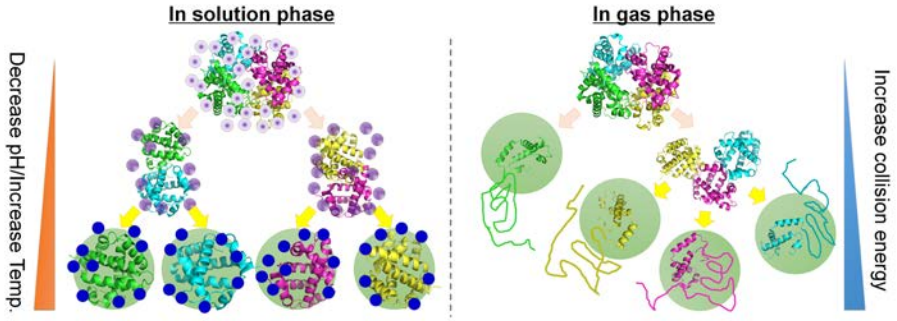

Scheme 1. Traditional disassembly pathway of Hb in solution and in gas phase. In solution, the disassembly is triggered by decreasing pH or increasing temperature. In gas phase, CID is initiated through energetic collisions with background gas. The striking difference is that the dimeric disassembly pathway is not observed during CID. Color markers: four subunits are labeled

with four different colors for clarity. For MPCs in solution, the solvent molecules are labeled with different colors to indicate different stress levels associated with changes in pH and temperature

Our control CID experiments of tetrameric Hb yielded monomeric globin chains, with no evidence of Hb dimer product ions, when ions under nESI from pure ammonium acetate solutions, as previously observed (**Figure 1A**) [3]. As expected, when we ramped the CID acceleration potential from 30 V to 70 V, we observed that the ratio of unfolded monomeric and trimeric Hb gradually increased in the tandem mass spectra, and again no dimeric Hb signals were observed (**Figure 1A**). Our results reveal that despite accounting for only approximately one quarter of Hb in terms of mass, the monomer species retained approximately half of the overall charge. This result agrees well with previously reported CID experiments for MPCs, in which the ejected monomer typically carries away a large percentage of the charge of the original complex [3, 24].

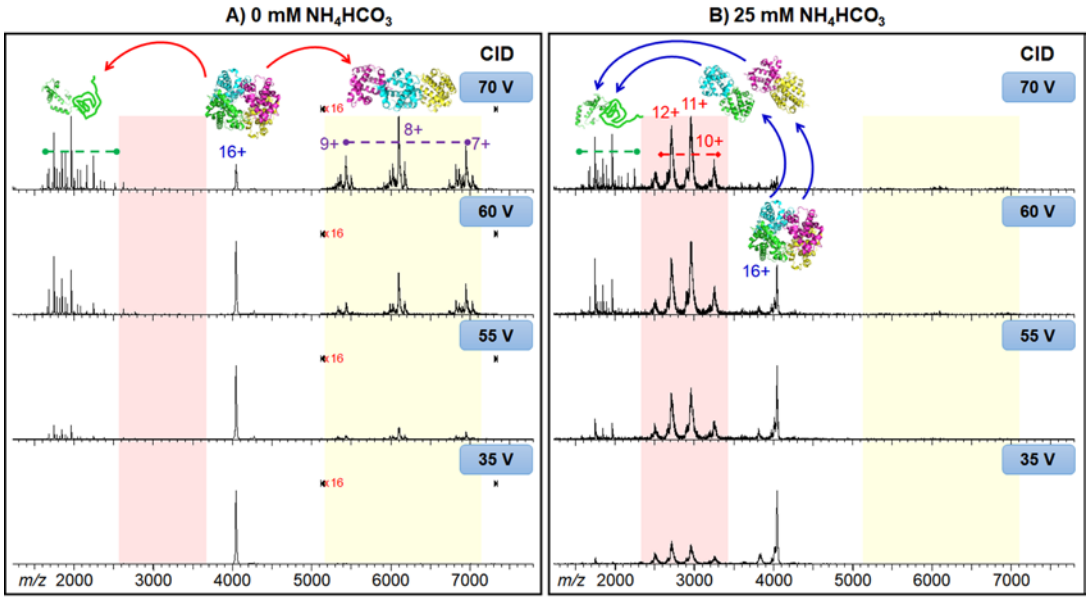

Figure 1. Electrospray of Hb from a NH_4HCO_3 solution alters the gas-phase dissociation pathway of Hb. The representative tandem MS spectra for tetrameric Hb CID from 35 V to 70 V without (**A**) or with NH_4HCO_3 (25 mM, **B**). Hb ions decay to form dimeric rather than monomeric product ions when produced from solutions containing NH_4HCO_3. All starting protein samples were buffered with 100 mM ammonium acetate (NH_4OAc). All experiments were performed with nanoESI, 1.5 kV. The spectra corresponding to trimer (*m/z* 5100-7100) in **A** were zoomed with 16 folds to make the details visible.

In order to capture dimeric Hb ions, we employed the gradual addition of NH_4HCO_3, and observed that the hetero-tetrameric Hb (αβαβ, 16+) adopted a dissociation pathway favoring the formation of heterodimeric Hb (primarily αβ without heme, 10+-12+). Detailed analysis of the different Hb forms produced under these conditions were also conducted, and revealed evidence of other expected Hb forms at lower levels (**Figure S1**). When we ramped the acceleration voltage used to initiate the CID experiment for Hb ions prepared in NH_4HCO_3, the relative amounts of dimeric product ions increased in a correlated fashion (**Figure 1B**). As expected, the extent of Hb fragmentation increases with the elevation of collision energy, and includes signals for monomeric Hb product ions, suggesting that CID of Hb ions produced from buffered NH_4HCO_3 solutions may also access the canonical asymmetric CID channel.

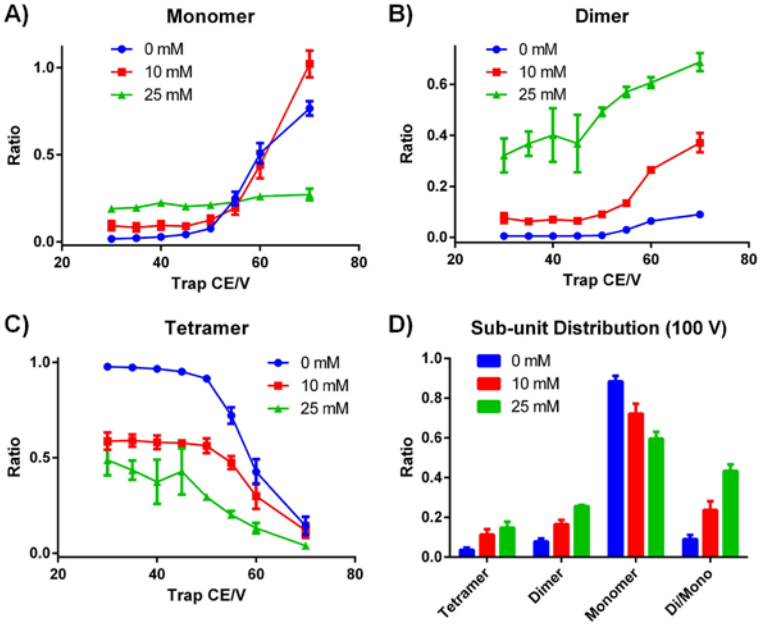

Figure 2. Quantitative characterization of the Hb tetramer ion CID pathway when prepared using NH_4HCO_3. Tandem MS results were obtained using tetrameric Hb 16+, with no precursor ion selection (all protein ions were subjected to CID) was applied. The monomeric (**A**), dimeric (**B**) and tetrameric globin (**C**) ratios generated by MS were plotted against the acceleration voltage used to initiate CID, and as a function of NH_4HCO_3 concentration. **D)** All Hb subunits change in terms of their relative intensities, and intensity ratios, with the gradual addition of NH_4HCO_3 in solution prior to IM-MS. Specifically, Tetramer amounts reported include only signal intensities for αβαβ; dimers include signals for αβ, αβ-heme, ββ-heme; and monomer amounts include signal intensities for α, α-heme, β and β-heme. All starting protein samples were buffered with 100 mM ammonium acetate (NH_4OAc). All error bars denote SD; n = 3.

We then moved to quantitatively characterize the effects of NH_4HCO_3 on the CID pathway of Hb tetramers. Results shown in **Figure 2** track the relative abundances of Hb parent ions along with the two main Hb product ion classes as a function of both acceleration potential and NH_4HCO_3 concentration in solution prior to nESI. Overall, we observed a greater amount of Hb dimer, and lesser amounts of Hb tetramer and monomer, as NH_4HCO_3 concentrations are increased (**Figures 2A-C**). MS data collected as a function of CID acceleration potential reveals decreased production of monomeric product ions from Hb tetramers prepared in NH_4HCO_3 (**Figure 2A**), and increased intensities for dimeric Hb ions (**Figure 2B**). Interestingly, we observe elevated amounts of Hb monomers and dimers for MS results recorded from NH_4HCO_3 containing solutions, indicating a disruption of Hb tetramers in solution. This observation correlates with the decreased relative amount of Hb tetramer observed from NH_4HCO_3 solutions (**Figure 2C**). The overall trends captured in our experiments are highlighted in **Figure 2D**, where clear positive correlations can be observed between CID acceleration potential, NH_4HCO_3 concentration, and dimeric Hb signal intensities. Taken together, these observations reveal that incubating Hb in bicarbonate solution prior to nESI facilitates the formation of dimeric Hb ions, which appear both prior to, and dramatically increase in intensity following, CID of Hb tetramer ions.

In order to decipher the underlying mechanism associated with our Hb observations, we sought to carry out a battery of tests on bicarbonate-containing Hb samples, as well as broaden our efforts to include additional protein complexes. To begin, we focused on studying the mass shifts and structural

changes induced in Hb tetramers upon treatment with NH_4HCO_3 [17-19]. Prior to our exploration of these details, a brief discussion highlighting the differences between our work and prior reports in this area is warranted. A number of previous reports have focused on using MS to analyze Hb subunit dynamics [4, 6, 39, 40] and contributed to the development of a bubble-induced unfolding mechanism [41] of proteins in bicarbonate-containing buffer. Subsequent efforts instead focused on electrothermal supercharging [42, 43] of small protein systems (e.g. ubiquitin and cytochrome c) produced from relatively concentrated NH_4HCO_3 solutions (e.g. mostly higher than 100 mM). Our prior efforts focused on probing the stabilizing effect of bound anions and cations on MPC structure [17-19], including NH_4HCO_3, which was used as an additive in acetate buffer at concentrations less than 10 mM, and classified as a modest stabilizing agent in the gas phase [19]. None of these prior studies have detected the dimer-based CID products as shown in **Figure 1**, nor focused on a study of gas-phase dissociation under conditions that include NH_4HCO_3 additives in solution.

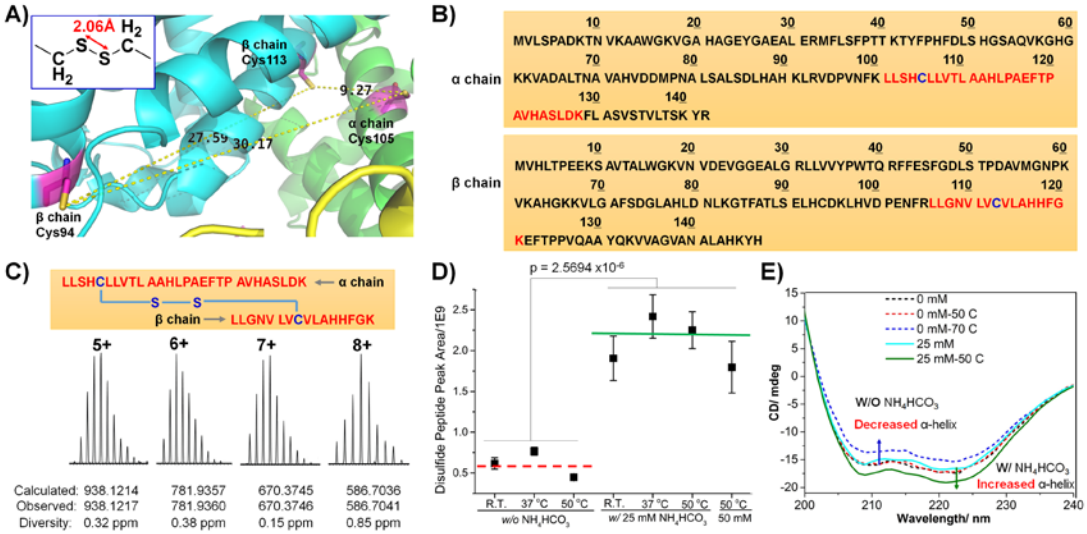

Figure 3. Disulfide bond formation catalyzed tracked by LC-MS/MS and spectroscopy. **A**) Zoomed view of the possible disulfide bonds among three cysteine residues in the α and β-chains of Hb (PDB ID: 1BZ0). The distances between each cysteine residues are labeled in angstroms (Å). The insert shows the typical S-S bond distance encountered in protein structures. **B**) Sequence for human Hb (Uniprot), shown for both the α and β chains. Possible tryptic fragments containing cysteines are marked with red (with blue indicating cysteine residues). **C**) Bottom-up nanoHPLC-MS-identified disulfide bonded peptide derived from trypsin digestion of bulk-heated Hb samples in the presence of bicarbonate. **D**) The peak areas for the signals identified in C as a function of various solution conditions. All error bars denote SD; n = 3. Statistical comparisons are based on Student's t-tests. **E**) CD spectra of bulk-heated Hb for different solution conditions.

In order to evaluate the underlying mechanism associated with the dimeric CID product ions observed in our data, we began by measuring the pH values (**Figure S2**) of the NH_4HCO_3-containing protein solutions used to collect data shown in Figures 1 and 2. Our results indicate that bicarbonate containing Hb solutions exhibit elevated pH values when compared with control solutions comprised of pure ammonium acetate. Interestingly, the pH value we recorded was elevated to a level approximating to the pKa value (8.18) of the cysteine residue upon the addition of NH_4HCO_3. This environment, therefore, likely promoted the deprotonation of cysteine residues within Hb.

To interrogate of the details of the chemical impact of NH_4HCO_3 on Hb structure, we performed a series of trypsin digestion experiments on Hb samples prepared in the presence of both bicarbonate and external heating, followed by bottom-up nanoHPLC-MS analysis. **Figure S3** shows representative

mass spectra for the bulk heated Hb using various bicarbonate buffer conditions. While extensive breakdown of tetrameric Hb can be readily reached throughout all concentrations of NH_4HCO_3 upon bulk heating, the gradual increase of dimeric Hb is also observed. **Figure 3A** shows the zoomed view of the possible sites of disulfide bond formation between the Hb α and β-chains (amino acid sequence information shown in **Figure 3B** is extracted from Uniprot for human Hb). As indicated, the typical S-S bond length is 2.06 Å, and the shortest distances identified in the Hb structure for inter-chain disulfide bond formation is between α-Cys105 and β-Cys113, having a distance of 9.27 Å. Such a bond formation event, therefore, must also be accompanied by fluctuations in the structure of the Hb tetramer in order to bring α-Cys105 and β-Cys113 within sufficient proximity for such bond formation. Our LC-MS results shown in **Figure 3C** identify a disulfide bonded tryptic peptide signal that contains α-Cys105 and β-Cys113. Quantitatively, data shown in **Figure 3D** indicates that the formation of a α-Cys105/β-Cys113 disulfide bond is highly dependent on the presence of NH_4HCO_3, statistically increasing in abundance by a factor of more than 2 (with p value < 0.0001, Figure 3D) upon its addition in solution. We also observe a small increase in disulfide bond formation upon modest heating of the solution, which appears optimized at 37°C. Surprisingly, circular dichroism (CD) results shown in **Figure 3E** indicated the increased amounts of α-helix within Hb in the presence of NH_4HCO_3 in bulk solution. Heating the sample with NH_4HCO_3 in solution further increases the Hb helix content, while rapid unfolding was observed by CD in the absence of NH_4HCO_3. It should be noted that more extensive heating, e.g. 70 °C, of Hb in the presence of NH_4HCO_3 leads to the unfolding of the protein.

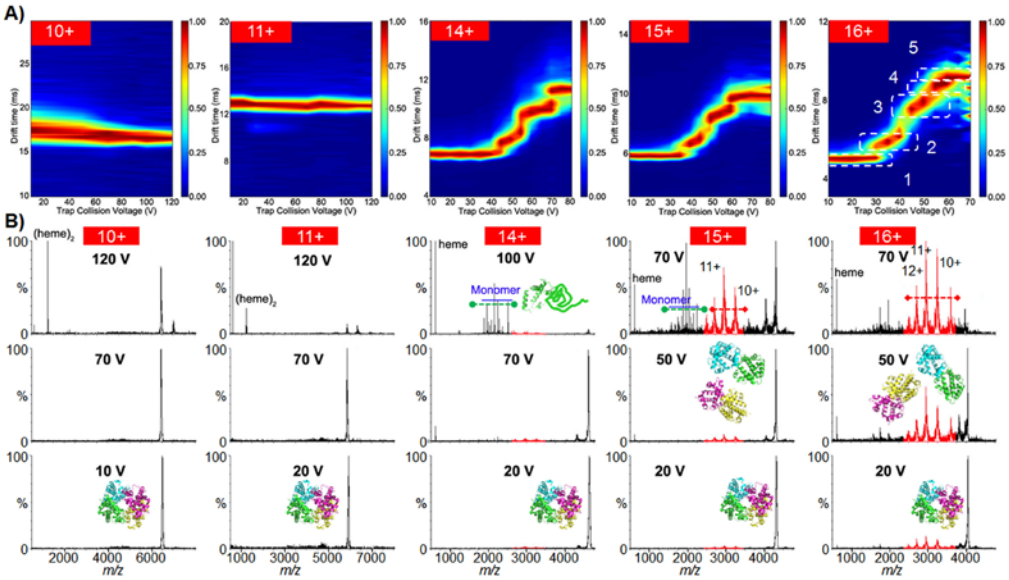

Figure 4. CIU reveals the level of gas-phase unfolding that accompanies Hb dimer ejection across a range of tetramer charge states (**A**) and corresponding tandem MS spectra (**B**). For all, buffer: NH_4OAc, 100 mM, NH_4HCO_3, 16 mM. For charge reduction (10+ and 11+), 10 mM triethylammonium acetate was added.

In order to investigate the amount of Hb unfolding that takes place during the CID process leading to dimeric product ions, we conducted CIU experiments on Hb tetramers prepared in bicarbonate-containing solutions over a wide range of charge states. Our results, shown in **Figure 4A**, indicate that dimer product ion formation occurs at acceleration voltage values (20 V) lower than the threshold energies required for Hb CIU (~40 V across three Hb charge states). Conversely, we also record CIU/CID data for lower Hb charge states where no clear CIU is observed, and CID product ions

are limited to heme ejection (**Figure 4B**). In addition, for higher charge states, extensive Hb tetramer unfolding, where up to 5 separate CIU features are detected over the energy range probed here, is observed under conditions where dimeric product ions represent most of the product ion current observed in our datasets (e.g. 50 V for 15+ and 16+, and 70 V for 14+). Furthermore, monomeric Hb product ion intensity increases dramatically at higher acceleration voltage, under conditions where Hb tetramer CIU has advanced significantly beyond its most compact state. Additionally, we calculated the CCSs for those dimeric Hb products, and turn out to be 2357 ± 17 Å^2, 2409 ± 48 Å^2, and 2629 ± 52 Å^2, for 10+, 11+ and 12+, respectively. These CCSs are not only comparable with IMPACT-predicted values (derived from PDB 2QSS; PA: 2165 Å^2; TJM: 2704 Å^2), but also well in accordance with previous reported native dimeric Hb CCSs (e.g. 11+, 2402 ± 100 Å^2) [44]. Taken together, our CIU data indicate that Hb unfolding is not required for Hb dimer product ion formation, but the production of dimer product ions is likely enhanced by the unfolding of Hb monomers at higher acceleration voltages.

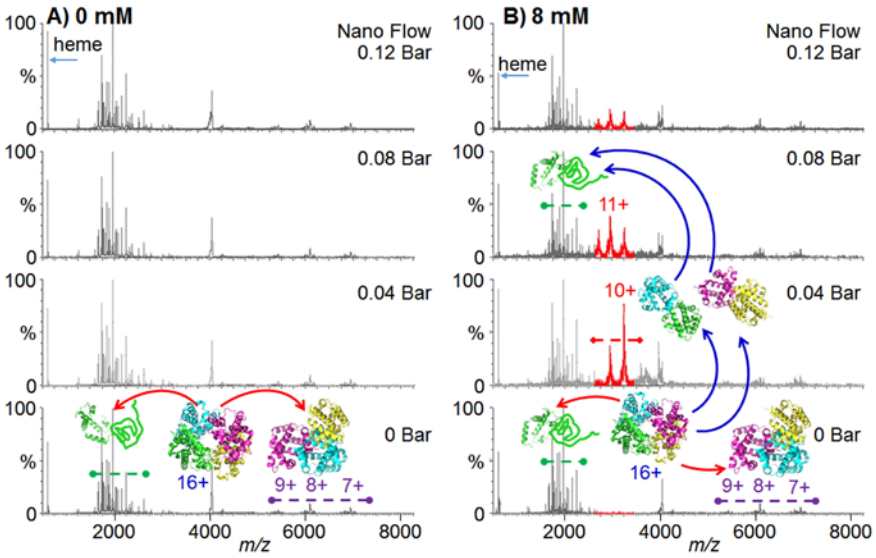

Figure 5. The flow rate used in nESI affects the efficiency of dimeric Hb product ion formation, as evidenced by representative tandem MS (trap CE, 70 V) spectra of Hb 16+ with NH_4HCO_3 at 0 mM (**A**) and 8 mM (**B**). All experiments were performed with nanoESI, 1.5 kV. All starting protein samples were buffered with 100 mM ammonium acetate (NH_4OAc).

We have also observed that the nESI flow rate used during our IM-MS experiments can significantly influence the amount of Hb dimer product ion produced from NH_4HCO_3 containing solutions (**Figure 5**). In the absence of NH_4HCO_3, Hb CID product ions include only the expected monomer and trimer (**Figure 5A**) and increasing the nanoflow backing pressure to produce higher nESI flow rates does not alter the product ion populations observed. In contrast, Hb CID product ions include significant dimer in the presence of NH_4HCO_3 in solution prior to nESI only when higher nESI flow rates utilized (**Figure 5B**). This evidence suggests that the disulfide bond formation detected in data shown in Figure 3 is dramatically accelerated when larger droplets are created during the nESI process, implicating the need for longer droplet lifetimes [45-48], and perhaps increased droplet heating [41, 43], as a means of initiating the bicarbonate-driven disulfide bonding chemistry that ultimately serves to alter Hb CID.

We have screened a number of additional salt additives, including nitrate (1+), tartrate (2+) and citrate (3+), for their ability to initiate similar disulfide bond formation chemistry in Hb [19]. However, as revealed in **Figure S4**, bicarbonate provides the only observable route in our experiments to form

dimeric Hb CID products . We further examined bicarbonate-driven disulfide bond formation chemistry using a glutathione (GSH), a model peptide frequently used to study disulfide bond formation.[49-51] Results shown in **Figure S5** clearly reveal evidence of disulfide bond formation in bicarbonate-containing solutions for GSH.

We also examined the CID pathway operative for a wide range of MPCs in the presence of bicarbonate, including avidin (**Figure S6**), transthyretin (TTR, **Figure S7**), concanavalin A (ConA, **Figures S8-12**), alcohol dehydrogenase (ADH, **Figure S13**) and glutamate dehydrogenase (GDH, **Figure S14**). Representative tandem mass spectra (**Figures S6c/7c**) clearly reveals asymmetric CID product ions including highly-charged monomers and charge-stripped oligomers deficient of a monomeric unit for avidin, ADH, and TTR upon the addition of NH_4HCO_3 in excess of those used in our Hb experiments. Interestingly, the high-resolution structures of avidin (PDB: 1VYO) and TTR (PDB ID: 1BMZ) (**Figures S6b/7b**), indicate no cysteine residues within sufficient proximity to form disulfide bonds between their respective monomers. As shown in **Figure S13b**, the high-resolution structural data for ADH (PDB: 1PIW) indicates the distance between the two closest cysteine residues within the structure to be 25.7 Å, a value significantly in excess of the analogous distance found in Hb. Similar to the tetramers discussed above, no sub-complexes were observed as CID products for bicarbonate-treated GDH (**Figure S14**). An analysis of the available high-resolution structure data (PDB ID of 3SBO) indicates that the two closest cysteine residues capable of linking two GDH monomers are 23.1 Å apart, a value of similar scale to that found in ADH and significantly larger than the distance found in our analysis of Hb. As such, data acquired for all of the above described complexes seems to comport with a rationale centered on the disulfide bonding of free cysteines within the Hb tetramer to explain the dimeric CID product ions observed for the complex upon the addition of bicarbonate to samples prior to nESI.

Notably, our data for the ConA tetramer represents an outlier from the mechanistic understanding described above. Our MS/MS data reveal that collisional activation of ConA tetramers treated with bicarbonate produce dimeric product ions similarly to Hb (**Figure S8**). Corresponding IM-MS data shown in **Figure S9** do indicate a structural compaction of ConA tetramer, possibly indicating the formation of a chemical cross-link within the structure. However, the ConA amino acid sequence and structure (PDB ID: 5CNA), shown in **Figure S10,** contain no cysteine residues, and thus the tetramer cannot form a disulfide bond as a means of producing the observed dimeric CID product ions. Similar to our investigations of Hb, we performed a series of bottom-up proteomic surveys of ConA samples incubated with bicarbonate additives and using solution heating (**Figures S10-12**). Our data reveals evidence of bicarbonate-dependent Gln and Asn deamination reactions. While a clear mechanistic explanation for dimeric ConA CID product ions is not revealed in these data, previous work [52] has highlighted the relatively sparse number of dimer-dimer contacts within the ConA quaternary structure, and it is conceivable that bicarbonate-initiated deamidation reactions would serve to weaken such contacts further either through structural changes or direct manipulation of interfacial residues. Prior work [16] has also shown that CID product ion formation can be directly influenced by the contact area between protein sub-complexes, thus providing a potential route for ConA dimer product ion formation that does require additional chemical bond formation. It is important to note, however, that the sequence coverage values achieved in proteomics survey (~40%) is insufficient to completely rule out the role of unknown chemical cross-linking reactions.

4. Conclusions

Here, we describe a set of observations and experiments that serve to further illuminate the mechanisms underpinning CID of MPCs. Our efforts focus on Hb, where we have extensively investigated an unexpected CID channel for the complex which is accessed through the addition of bicarbonate to Hb samples prior to nESI. We find that ammonium bicarbonate present within a more concentrated ammonium acetate solution has the potential to chemically modify MPCs, creating at least one disulfide linkage within the tetramer, which leads to dimeric product ions following collisional activation. Bicarbonate has been previously used for the chemical creation of disulfide bonds (typically added as $KHCO_3$), and acts to deprotonate thiols, further promoted under basic conditions [53-55]. Typical chemical disulfide bond creation requires the addition of a leaving group (e.g. Br_2) to the reaction mixture, and the identity of this entity is currently unknown under our experimental conditions. Despite this, we find that the NH_4HCO_3 additives promote the disulfide bond formation in MPCs and peptides readily, and do so with improved fidelity upon heating. Furthermore, it is likely that the chemistry we identify is operative in nESI droplets, favoring larger droplets which adopt longer lifetimes and larger heating potential. Notably, prior work from Cooks[56, 57] and Zare [58], indicate that microdroplet-based chemical crosslinking reactions between proximal cysteine residues may subjected to increased reaction kinetics when compared to similar reactions carried out in solution. Within MPCs, our efforts have indicated that cystines separated by over ~ 9 Å within the high-resolution protein structure can be bridged under these conditions, supporting the notion that such chemistry could be used to study the dynamics of MPCs under a variety of conditions.

Our experiments examined a wide range of MPCs and found that most assemblies do not respond with altered CID product ions upon treatment with bicarbonate, likely due to the native distances associated with the available cysteine residues in their sequences. The exception in these observations is ConA, where we surmise that a series of deamidation reactions caused by bicarbonate addition and heating may destabilize the dimer-dimer interface sufficiently to produce dimer product ions upon collisional activation in the gas phase, but our experiments cannot rule out potential chemical crosslinks that may form under our conditions. Overall, our dataset adds substantially to the growing catalog of MPC CID efforts that have identified dissociation pathways that produce subcomplex product ions that can be generated upon the alteration of protein charge state [15, 59-61], inter-subunit contact area [16], and disulfide bonding status [62]. In addition, our efforts contribute to the growing interest in gas-phase dissociation processes that link directly to MPC organization and topology [63-65]. Future efforts will be directed toward the production of MS methods that leverage chemical modifications and CID for the elucidation of MPC structure.

ACKNOWLEDGMENT

GL thanks the funding support for a Postdoctoral Career Development Award provided by the American Society for Mass Spectrometry (2019), the USTC Graduate School Fellowship for International Exchange (GS006), the Fundamental Research Funds for the Central Universities (USTC, WK6030000026) and the Fundamental Research Funds for the Central Universities (China, 020-63213057). GH acknowledges National Natural Science Foundation of China (21475121 and 21475121), the Fundamental Research Funds for the Central Universities (WK3460000002), the Innovative Program of Development Foundation of Hefei Center for Physical Science and Technology (2017FXCX003), and Recruitment Program of Global Expert. LL acknowledges a Vilas Distinguished Achievement Professorship and Charles Melbourne Johnson Distinguished Chair Professorship with funding provided by the Wisconsin Alumni Research Foundation and University of Wisconsin-Madison

School of Pharmacy and the funding support of this work partly by NIH (R01DK071801, R56DK071801, and RF1AG052324), and NSF (CHE-1710140). BTR thanks the National Science Foundation Division of Chemistry under Grant 1808541 (with co-funding from the Division of Molecular and Cellular Biosciences) for their support of this work.

Abbreviations: αβαβ, tetrameric Hb; αβ, holo-dimeric globin; αβ-heme, apo-dimeric globin; ββ-heme, apo-dimeric globin; α, holo-α-globin; β, holo-β-globin; α-heme, apo-α-globin; β-heme, apo-β-globin.

REFERENCES

1. Bosch, X.; Poch, E.; Grau, J. M., Rhabdomyolysis and acute kidney injury. *N. Engl. J. Med.* **2009,** *361* (1), 62-72.

2. Pillai, A. S.; Chandler, S. A.; Liu, Y.; Signore, A. V.; Cortez-Romero, C. R.; Benesch, J. L. P.; Laganowsky, A.; Storz, J. F.; Hochberg, G. K. A.; Thornton, J. W., Origin of complexity in haemoglobin evolution. *Nature* **2020,** *581* (7809), 480-485.

3. Versluis, C.; Heck, A. J. R., Gas-phase dissociation of hemoglobin. *Int. J. Mass spectrom.* **2001,** *210–211*, 637-649.

4. Boys, B. L.; Kuprowski, M. C.; Konermann, L., Symmetric behavior of hemoglobin alpha- and beta- subunits during acid-induced denaturation observed by electrospray mass spectrometry. *Biochemistry* **2007,** *46* (37), 10675-10684.

5. Griffith, W. P.; Kaltashov, I. A., Highly asymmetric interactions between globin chains during hemoglobin assembly revealed by electrospray ionization mass spectrometry. *Biochemistry* **2003,** *42* (33), 10024-33.

6. Liu, J.; Konermann, L., Cation-induced stabilization of protein complexes in the gas phase: mechanistic insights from hemoglobin dissociation studies. *J. Am. Soc. Mass Spectrom.* **2014,** *25* (4), 595-603.

7. Kang, Y.; Douglas, D. J., Gas-phase ions of human hemoglobin A, F, and S. *J. Am. Soc. Mass Spectrom.* **2011,** *22* (7), 1187-1196.

8. Laganowsky, A.; Reading, E.; Allison, T. M.; Ulmschneider, M. B.; Degiacomi, M. T.; Baldwin, A. J.; Robinson, C. V., Membrane proteins bind lipids selectively to modulate their structure and function. *Nature* **2014,** *510* (7503), 172-175.

9. Snijder, J.; Rose, R. J.; Veesler, D.; Johnson, J. E.; Heck, A. J., Studying 18 MDa virus assemblies with native mass spectrometry. *Angew. Chem. Int. Ed.* **2013,** *52* (14), 4020-4023.

10. Benesch, J. L.; Robinson, C. V., Mass spectrometry of macromolecular assemblies: preservation and dissociation. *Curr. Opin. Struct. Biol.* **2006,** *16* (2), 245-251.

11. Wilm, M.; Shevchenko, A.; Houthaeve, T.; Breit, S.; Schweigerer, L.; Fotsis, T.; Mann, M., Femtomole sequencing of proteins from polyacrylamide gels by nano-electrospray mass spectrometry. *Nature* **1996,** *379* (6564), 466-469.

12. Ruotolo, B. T.; Giles, K.; Campuzano, I.; Sandercock, A. M.; Bateman, R. H.; Robinson, C. V., Evidence for macromolecular protein rings in the absence of bulk water. *Science* **2005,** *310* (5754), 1658-1661.

13. Zhong, Y.; Han, L.; Ruotolo, B. T., Collisional and Coulombic unfolding of gas-phase proteins: high correlation to their domain structures in solution. *Angew. Chem. Int. Ed.* **2014,** *53* (35), 9209-9212.

14. Dixit, S. M.; Polasky, D. A.; Ruotolo, B. T., Collision induced unfolding of isolated proteins in the

gas phase: past, present, and future. *Curr. Opin. Chem. Biol.* **2018,** *42*, 93-100.
15. Pagel, K.; Hyung, S. J.; Ruotolo, B. T.; Robinson, C. V., Alternate dissociation pathways identified in charge-reduced protein complex ions. *Anal. Chem.* **2010,** *82* (12), 5363-5372.
16. Han, L.; Ruotolo, B. T., Ion Mobility-Mass Spectrometry Differentiates Protein Quaternary Structures Formed in Solution and in Electrospray Droplets. *Anal. Chem.* **2015,** *87* (13), 6808-6013.
17. Han, L.; Ruotolo, B. T., Hofmeister salts recover a misfolded multiprotein complex for subsequent structural measurements in the gas phase. *Angew. Chem. Int. Ed.* **2013,** *52* (32), 8329-8332.
18. Han, L.; Hyung, S. J.; Ruotolo, B. T., Bound cations significantly stabilize the structure of multiprotein complexes in the gas phase. *Angew. Chem. Int. Ed.* **2012,** *51* (23), 5692-5695.
19. Han, L.; Hyung, S. J.; Mayers, J. J.; Ruotolo, B. T., Bound anions differentially stabilize multiprotein complexes in the absence of bulk solvent. *J. Am. Chem. Soc.* **2011,** *133* (29), 11358-11367.
20. Zhang, H.; Lu, H.; Chingin, K.; Chen, H., Stabilization of Proteins and Noncovalent Protein Complexes during Electrospray Ionization by Amino Acid Additives. *Anal. Chem.* **2015,** *87* (14), 7433-7438.
21. Li, G.; Yuan, S.; Zheng, S.; Chen, Y.; Zheng, Z.; Liu, Y.; Huang, G., The Effect of Salts in Promoting Specific and Competitive Interactions between Zinc Finger Proteins and Metals. *J. Am. Soc. Mass Spectrom.* **2017,** *28* (12), 2658-2664.
22. Breuker, K.; McLafferty, F. W., Stepwise evolution of protein native structure with electrospray into the gas phase, 10(-12) to 10(2) s. *Proc. Natl. Acad. Sci. U. S. A.* **2008,** *105* (47), 18145-18152.
23. Hall, Z.; Politis, A.; Bush, M. F.; Smith, L. J.; Robinson, C. V., Charge-state dependent compaction and dissociation of protein complexes: insights from ion mobility and molecular dynamics. *J. Am. Chem. Soc.* **2012,** *134* (7), 3429-3438.
24. Jones, C. M.; Beardsley, R. L.; Galhena, A. S.; Dagan, S.; Cheng, G.; Wysocki, V. H., Symmetrical gas-phase dissociation of noncovalent protein complexes via surface collisions. *J. Am. Chem. Soc.* **2006,** *128* (47), 15044-15045.
25. Kao, A.; Chiu, C. L.; Vellucci, D.; Yang, Y.; Patel, V. R.; Guan, S.; Randall, A.; Baldi, P.; Rychnovsky, S. D.; Huang, L., Development of a novel cross-linking strategy for fast and accurate identification of cross-linked peptides of protein complexes. *Mol. Cell. Proteomics* **2011,** *10* (1), M110 002212.
26. Liu, F.; Rijkers, D. T.; Post, H.; Heck, A. J., Proteome-wide profiling of protein assemblies by cross-linking mass spectrometry. *Nat. Methods* **2015,** *12* (12), 1179-84.
27. Sinz, A., Cross-Linking/Mass Spectrometry for Studying Protein Structures and Protein-Protein Interactions: Where Are We Now and Where Should We Go from Here? *Angew. Chem. Int. Ed.* **2018,** *57* (22), 6390-6396.
28. Hanozin, E.; Grifnee, E.; Gattuso, H.; Matagne, A.; Morsa, D.; Pauw, E., Covalent Cross-Linking as an Enabler for Structural Mass Spectrometry. *Anal. Chem.* **2019,** *91* (20), 12808-12818.
29. Iacobucci, C.; Piotrowski, C.; Aebersold, R.; Amaral, B. C.; Andrews, P.; Bernfur, K.; Borchers, C.; Brodie, N. I.; Bruce, J. E.; Cao, Y.; Chaignepain, S.; Chavez, J. D.; Claverol, S.; Cox, J.; Davis, T.; Degliesposti, G.; Dong, M. Q.; Edinger, N.; Emanuelsson, C.; Gay, M.; Gotze, M.; Gomes-Neto, F.; Gozzo, F. C.; Gutierrez, C.; Haupt, C.; Heck, A. J. R.; Herzog, F.; Huang, L.; Hoopmann, M. R.; Kalisman, N.; Klykov, O.; Kukacka, Z.; Liu, F.; MacCoss, M. J.; Mechtler, K.; Mesika, R.; Moritz, R. L.; Nagaraj, N.; Nesati, V.; Neves-Ferreira, A. G. C.;

Ninnis, R.; Novak, P.; O'Reilly, F. J.; Pelzing, M.; Petrotchenko, E.; Piersimoni, L.; Plasencia, M.; Pukala, T.; Rand, K. D.; Rappsilber, J.; Reichmann, D.; Sailer, C.; Sarnowski, C. P.; Scheltema, R. A.; Schmidt, C.; Schriemer, D. C.; Shi, Y.; Skehel, J. M.; Slavin, M.; Sobott, F.; Solis-Mezarino, V.; Stephanowitz, H.; Stengel, F.; Stieger, C. E.; Trabjerg, E.; Trnka, M.; Vilaseca, M.; Viner, R.; Xiang, Y.; Yilmaz, S.; Zelter, A.; Ziemianowicz, D.; Leitner, A.; Sinz, A., First Community-Wide, Comparative Cross-Linking Mass Spectrometry Study. *Anal. Chem.* **2019,** *91* (11), 6953-6961.

30. Gutierrez, C. B.; Block, S. A.; Yu, C.; Soohoo, S. M.; Huszagh, A. S.; Rychnovsky, S. D.; Huang, L., Development of a Novel Sulfoxide-Containing MS-Cleavable Homobifunctional Cysteine-Reactive Cross-Linker for Studying Protein-Protein Interactions. *Anal. Chem.* **2018,** *90* (12), 7600-7607.

31. Samulak, B. M.; Niu, S.; Andrews, P. C.; Ruotolo, B. T., Ion Mobility-Mass Spectrometry Analysis of Cross-Linked Intact Multiprotein Complexes: Enhanced Gas-Phase Stabilities and Altered Dissociation Pathways. *Anal. Chem.* **2016,** *88* (10), 5290-5298.

32. Polasky, D. A.; Lermyte, F.; Nshanian, M.; Sobott, F.; Andrews, P. C.; Loo, J. A.; Ruotolo, B. T., Fixed-Charge Trimethyl Pyrilium Modification for Enabling Enhanced Top-Down Mass Spectrometry Sequencing of Intact Protein Complexes. *Anal. Chem.* **2018,** *90* (4), 2756-2764.

33. Polasky, D. A.; Dixit, S. M.; Keating, M. F.; Gadkari, V. V.; Andrews, P. C.; Ruotolo, B. T., Pervasive Charge Solvation Permeates Native-like Protein Ions and Dramatically Influences Top-down Sequencing Data. *J. Am. Chem. Soc.* **2020,** *142* (14), 6750-6760.

34. Ruotolo, B. T.; Benesch, J. L.; Sandercock, A. M.; Hyung, S. J.; Robinson, C. V., Ion mobility-mass spectrometry analysis of large protein complexes. *Nat. Protoc.* **2008,** *3* (7), 1139-1152.

35. Bush, M. F.; Hall, Z.; Giles, K.; Hoyes, J.; Robinson, C. V.; Ruotolo, B. T., Collision Cross Sections of Proteins and Their Complexes: A Calibration Framework and Database for Gas-Phase Structural Biology. *Anal. Chem.* **2010,** *82* (22), 9557-9565.

36. Eschweiler, J. D.; Rabuck-Gibbons, J. N.; Tian, Y.; Ruotolo, B. T., CIUSuite: A Quantitative Analysis Package for Collision Induced Unfolding Measurements of Gas-Phase Protein Ions. *Anal. Chem.* **2015,** *87* (22), 11516-11522.

37. Abaturov, L. V.; Molchanova, T. P.; Nosova, N. G.; Shlyapnikov, S. V.; Faizullin, D. A., Conformational dynamics of the tetrameric hemoglobin molecule as revealed by hydrogen exchange: 2. Effect of intersubunit contact cleavage. *Mol. Biol.* **2006,** *40* (3), 413-426.

38. Lukin, J. A.; Ho, C., The structure--function relationship of hemoglobin in solution at atomic resolution. *Chem. Rev.* **2004,** *104* (3), 1219-1230.

39. Simmons, D. A.; Wilson, D. J.; Lajoie, G. A.; Doherty-Kirby, A.; Konermann, L., Subunit disassembly and unfolding kinetics of hemoglobin studied by time-resolved electrospray mass spectrometry. *Biochemistry* **2004,** *43* (46), 14792-801.

40. Sowole, M. A.; Vuong, S.; Konermann, L., Interactions of hemoglobin and myoglobin with their ligands CN(-), CO, and O2 monitored by electrospray ionization-mass spectrometry. *Anal. Chem.* **2015,** *87* (19), 9538-9545.

41. Hedges, J. B.; Vahidi, S.; Yue, X.; Konermann, L., Effects of ammonium bicarbonate on the electrospray mass spectra of proteins: evidence for bubble-induced unfolding. *Anal. Chem.* **2013,** *85* (13), 6469-76.

42. Cassou, C. A.; Williams, E. R., Anions in electrothermal supercharging of proteins with electrospray ionization follow a reverse Hofmeister series. *Anal. Chem.* **2014,** *86* (3), 1640-1647.

43. Sterling, H. J.; Cassou, C. A.; Susa, A. C.; Williams, E. R., Electrothermal supercharging of proteins in native electrospray ionization. *Anal. Chem.* **2012,** *84* (8), 3795-3801.
44. Kang, Y.; Terrier, P.; Douglas, D. J., Mass Spectra and Ion Collision Cross Sections of Hemoglobin. *J. Am. Soc. Mass Spectrom.* **2011,** *22* (2), 290-299.
45. Song, H.; Ismagilov, R. F., Millisecond Kinetics on a Microfluidic Chip Using Nanoliters of Reagents. *J. Am. Chem. Soc.* **2003,** *125* (47), 14613-14619.
46. Theberge, A. B.; Courtois, F.; Schaerli, Y.; Fischlechner, M.; Abell, C.; Hollfelder, F.; Huck, W. T. S., Microdroplets in Microfluidics: An Evolving Platform for Discoveries in Chemistry and Biology. *Angew. Chem. Int. Ed.* **2010,** *49* (34), 5846-5868.
47. Kaminski, T. S.; Garstecki, P., Controlled droplet microfluidic systems for multistep chemical and biological assays. *Chem. Soc. Rev.* **2017,** *46* (20), 6210-6226.
48. Mortensen, D. N.; Williams, E. R., Ultrafast (1 mus) Mixing and Fast Protein Folding in Nanodrops Monitored by Mass Spectrometry. *J. Am. Chem. Soc.* **2016,** *138* (10), 3453-3460.
49. Li, G.; Pei, J.; Yin, Y.; Huang, G., Direct sequencing of a disulfide-linked peptide with electrospray ionization tandem mass spectrometry. *Analyst* **2015,** *140* (8), 2623-2627.
50. Li, G.; Yin, Y.; Huang, G., Increased disulfide peptide sequence coverage via “cleavage ON/OFF” switch during nanoelectrospray. *RSC Adv.* **2014,** *4* (103), 59650-59654.
51. Xia, Y.; Cooks, R. G., Plasma induced oxidative cleavage of disulfide bonds in polypeptides during nanoelectrospray ionization. *Anal. Chem.* **2010,** *82* (7), 2856-2864.
52. Zhong, Y.; Feng, J.; Ruotolo, B. T., Robotically assisted titration coupled to ion mobility-mass spectrometry reveals the interface structures and analysis parameters critical for multiprotein topology mapping. *Anal. Chem.* **2013,** *85* (23), 11360-11368.
53. Hogg, P. J., Disulfide bonds as switches for protein function. *Trends Biochem. Sci.* **2003,** *28* (4), 210-214.
54. Xiao, H.; Chen, J.; Liu, M.; Wu, H.; Ding, J., An Approach to Disulfide Synthesis Promoted by Sulfonyl Chloride in Sodium Bicarbonate Aqueous Media. *Phosphorus, Sulfur, Silicon Relat. Elem.* **2009,** *184* (10), 2553-2559.
55. Bayer, M.; Konig, S., Abundant cysteine side reactions in traditional buffers interfere with the analysis of posttranslational modifications and protein quantification - How to compromise. *Rapid Commun. Mass Spectrom.* **2016,** *30* (15), 1823-1828.
56. Marsh, B. M.; Iyer, K.; Cooks, R. G., Reaction Acceleration in Electrospray Droplets: Size, Distance, and Surfactant Effects. *J. Am. Soc. Mass Spectrom.* **2019,** *30* (10), 2022-2030.
57. Wei, Z.; Wleklinski, M.; Ferreira, C.; Cooks, R. G., Reaction Acceleration in Thin Films with Continuous Product Deposition for Organic Synthesis. *Angew. Chem. Int. Ed.* **2017,** *56* (32), 9386-9390.
58. Lee, J. K.; Banerjee, S.; Nam, H. G.; Zare, R. N., Acceleration of reaction in charged microdroplets. *Q. Rev. Biophys.* **2015,** *48* (4), 437-444.
59. Erba, E. B.; Ruotolo, B. T.; Barsky, D.; Robinson, C. V., Ion Mobility-Mass Spectrometry Reveals the Influence of Subunit Packing and Charge on the Dissociation of Multiprotein Complexes. *Anal. Chem.* **2010,** *82* (23), 9702-9710.
60. Bornschein, R. E.; Ruotolo, B. T., Ion mobility-mass spectrometry of charge-reduced protein complexes reveals general trends in the collisional ejection of compact subunits. *Analyst* **2015,** *140* (20), 7020-7029.
61. Bornschein, R. E.; Niu, S.; Eschweiler, J.; Ruotolo, B. T., Ion Mobility-Mass Spectrometry Reveals Highly-Compact Intermediates in the Collision Induced Dissociation of Charge-Reduced Protein

Complexes. *J. Am. Soc. Mass Spectrom.* **2016,** *27* (1), 41-49.
62. Aquilina, J. A., The major toxin from the Australian Common Brown Snake is a hexamer with unusual gas-phase dissociation properties. *Proteins* **2009,** *75* (2), 478-485.
63. Snyder, D. T.; Panczyk, E. M.; Somogyi, A.; Kaplan, D. A.; Wysocki, V., Simple and Minimally Invasive SID Devices for Native Mass Spectrometry. *Anal. Chem.* **2020,** *92* (16), 11195-11203.
64. VanAernum, Z. L.; Gilbert, J. D.; Belov, M. E.; Makarov, A. A.; Horning, S. R.; Wysocki, V. H., Surface-Induced Dissociation of Noncovalent Protein Complexes in an Extended Mass Range Orbitrap Mass Spectrometer. *Anal. Chem.* **2019,** *91* (5), 3611-3618.
65. Snyder, D. T.; Panczyk, E.; Stiving, A. Q.; Gilbert, J. D.; Somogyi, A.; Kaplan, D.; Wysocki, V., Design and Performance of a Second-Generation Surface-Induced Dissociation Cell for Fourier Transform Ion Cyclotron Resonance Mass Spectrometry of Native Protein Complexes. *Anal. Chem.* **2019,** *91* (21), 14049-14057.